Available online at www.sciencedirect.com
ScienceDirect
Experimental Thermal and Fluid Science 31 (2007) 579–592
Experimental Thermal and Fluid Science
www.elsevier.com/locate/etfs

Characterization of the flow field and stratification effects of fuel spray in a visualization engine using DPIV and entropy analysis

K.H. Lee, C.H. Lee *

Department of Mechanical Engineering, Hanyang University, 1271 Sa 1-dong, Ansan, Kyounggi-do, Republic of Korea

Received 19 March 2006; received in revised form 9 June 2006; accepted 13 June 2006

Abstract

The objective of this study was to analyze the spray characteristics according to the injection duration under ambient pressure conditions and the injection timing in the visualization engine. In order to investigate spray behavior, the spray velocity is obtained through the PIV method a useful optical diagnostics technology and the vorticity calculated from the spray velocity component. These results elucidated the relationship between vorticity and entropy which plays an important role in the diffusion process for early injection and the stratification process for late injection cases. In addition, the homogeneous diffusion rate of spray was quantified using the entropy analysis based on Boltzmann's statistical thermodynamics. Using these methods, it was found that the homogeneous mixture distribution is more effective as a momentum dissipation of surrounding air than that of the spray concentration to increase the injection timing. It is found that the homogenous diffusion rate increased as the injection timing moved to the early intake stroke process, and BTDC 60° was the most efficient injection timing for the stratified mixture formation during the compression stroke.

Keywords: PIV technique; Entropy analysis; Stratification degree; Vorticity; Direct injection spark ignition(DISI) engine

1. Introduction

As the environmental problems caused by vehicle exhaust emissions have become more severe, exhaust emission standards and fuel economy regulations have become more stringent. For the gasoline engine, the emission of CO_2 gas, which is one of the main causes of global warming, has become a severe problem along with the emission of toxic gases such as CO, HC, and NO_x. Recently, the GDI (gasoline direct injection) engine has been spotlighted as the next generation engine that can satisfy the SULEV (Super Ultra Low Emission Vehicle) regulations and reduce fuel consumption. Thus, studies of a high-pressure, vortex-type injector, one of the key parts in the development of the GDI engine, have been performed by many researchers [19–25].

Zhao et al. visualized the development process of the fuel spray of the GDI injector by using a two-dimensional Mie scattering method while measuring the SMD (Sauter mean diameter) and the velocity of spray to investigate the evaporation of fuel [24]. Yamauchi et al. performed a numerical analysis on the fuel spray vortex of a high-pressure GDI injector by using a GTT (Generalized Tank and Tube) code, and comparing the results with those obtained by PDA [25]. In fact, while many other studies have investigated the characteristics of fuel injector sprays, the experimental difficulties of obtaining detailed information, have limited the amount of information available on spray structure and the characteristics of the GDI injector.

Yamakawa et al. developed a new fuel spray measurement technology known as, LIF-PIV (Laser induced fluorescence-particle image velocimetry), to measure the velocity of fuel spray induced airflow with variations in the ambient pressure [8]. They investigated particle diameters, velocity distribution, and the evaporation process of the spray. Yuyama [26] and Chikahisa [27] developed a

* Corresponding author. Tel.: +82 31 418 9293; fax: +82 31 406 5550.
E-mail address: leemech@encod.hanyang.ac.kr (C.H. Lee).

0894-1777/$ - see front matter © 2006 Elsevier Inc. All rights reserved.
doi:10.1016/j.expthermflusci.2006.06.003

Nomenclature

S^*	dimensionless entropy value	I_{max}	the maximum intensity in a cell
M	number of cells in an image	I_i	image intensity of a cell (0–255)
I_t	integrated value of the image intensity over the whole image area	κ	Boltzmann constant
		ω	vorticity (1/s)

new entropy analysis method based on statistical thermodynamics and applied this method to the investigation of the propagation process of diesel spray [27,29,30]. However, these previous studies indicate that there is still much uncertainty about the mixing process of gasoline-direct injectors. From this point of view, a more exact investigation of the mixture formation and the correlation between spray and induced air is required.

The present study developed a laser scattering image detection system, and measured the macro-scale fuel spray characteristics such as spray penetration length and spray angle. An entropy analysis method based on the concept of statistical thermodynamics has been developed, and the mixture formation process was analyzed using this method. Cross-correlation DPIV [1–19] has been developed, and the velocity distribution of the GDI fuel particle has been investigated in the visualization engine. And, using entropy analysis, the stratification degree near the spark plug has been investigated.

2. Experimental setup and methods

2.1. Experimental setup and proceedings

Fig. 1 shows the visualization system used to obtain the mixture distribution in the cylinder for simulating intake stroke in accordance with the changing intake flow field. A Nd:YAG laser (Contiuum Surelite I–10) was used as a light source, and the maximum power and wavelength was 200 mJ and 532 nm, respectively. The thickness of the induced-laser sheet beam was 500 μm. The exposure time of the CCD camera, the illumination time of the laser beam, and the injection time of the fuel spray were controlled by a timing board (PC-TIO-10) and the LabView program. By controlling the laser trigger signal and delay timing, scattering images of fuel spray could be obtained through the image board (frame grabber, metio II/digital) of a computer by using a high-resolution CCD camera manufactured by the Kodak Co. (1008 × 1018, Megaplus ES 1.0). Also, we used a pulse generator (DG535, SRS), which can be controlled by pico units.

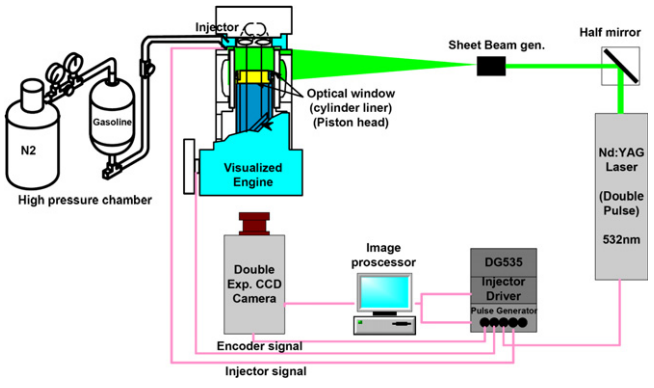

Fig. 1. Schematic diagram of optical visual engine system.

The particles are illuminated with a 1 mm thin light sheet, delivered from an Nd:YAG laser through a combination of sheet beam generator with spherical and cylindrical lens. Since only a fraction of 1/10 of the maximum power of the laser (100 mJ) is employed in the final beam. One individual image frame or a sequence of up to 30 images of the flow can be captured with a CCD camera, mounted perpendicular to the light sheet and connected to a computer via a frame grabber. The camera requires that the laser produces two pulses on every second frame in order to achieve optimum image quality. The entire system is synchronized using the composite video output signal extracted from the camera, which represents the input of the control circuit. The schematic connections of the system components and timing chart are shown in Figs. 1 and 5, respectively. The specifications of the visualization engine and injector are shown in Tables 1 and 2. Table 3 shows the characteristic specification of the test injector.

Table 1
Specification of engine

Item	Specification
Engine	4 valve DOHC single cylinder
Fuel	Gasoline
Clearance volume	47.3 cc
Bore × Stroke	81 mm × 88 mm
Compression ratio	10.3
Operation speed (rpm)	600

Table 2
Specification of GDI injectors

Factor injector	Injection pressure	Spray pattern	Offset angle	Swirl
M	5 MPa	Hollow cone	0°	o

Table 3
Specification of test injectors

Type	θ_0 (spray angle)	Injector hole	Inj. Rate
Swirl	$\theta_0 = 60°$	0.5 (mm)	10 (mg)

Fig. 2(a) shows the schematic diagram of the injector attached angle and optical window. The cylinder liner and piston are composed of quartz (fused silica). The fuel spray formation process and the mixture distribution in a single cylinder visualization engine were observed. A schematic diagram of the laser beam system is shown in Fig. 1. The laser sheet beam was illuminated into the cylinder liner or the transparent piston crown. A rotary encoder is mounted at the camshaft, and the injection timing and the ICCD are synchronized with the encoder signal. The spray images were obtained at various crankshaft angles during the intake stroke, and then the spray velocity and vorticity were calculated using the PIV and vorticity algorithms. Fig. 2(b) shows the schematic diagram of swirl type injectors used in this experiment.

The measurement system of the mixture formation at the late injection mode is shown in Fig. 3. To analyze the stratification effect near the spark plug at the late injection mode, the laser sheet beam was illuminated on a horizontal cross-section plane near the spark plug. Optical accesses

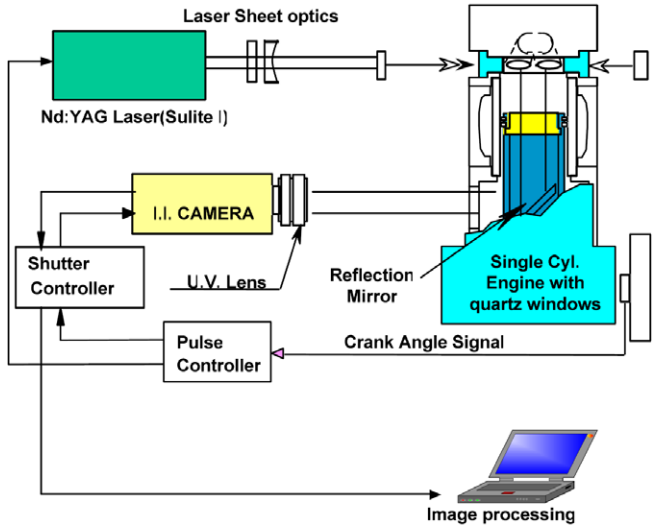

Fig. 3. Measurement system of the mixture distribution for the late injection mode.

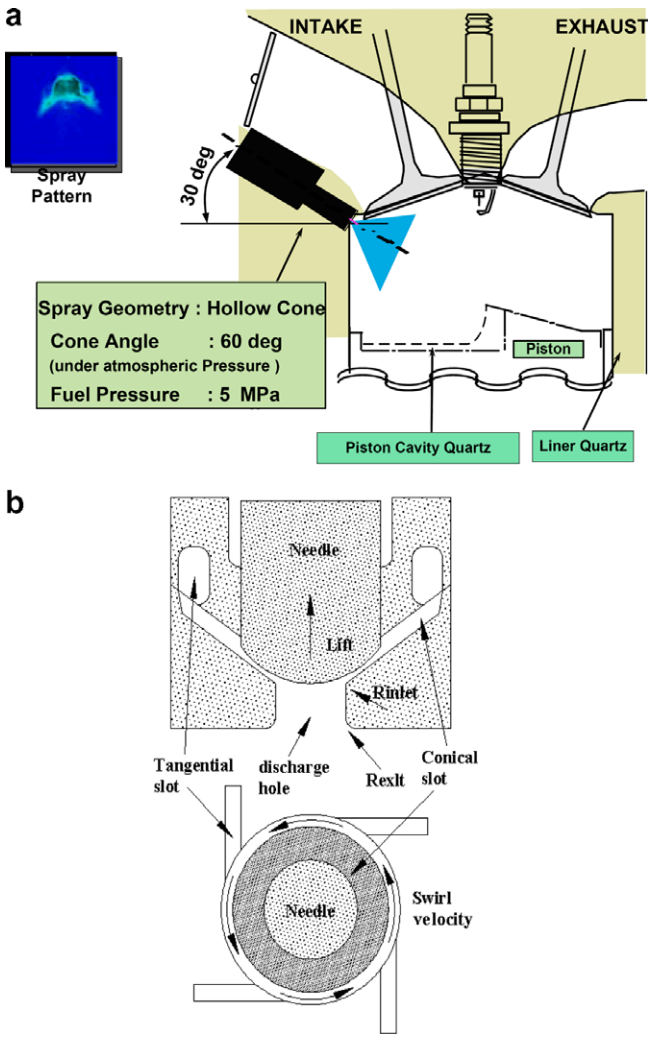

Fig. 2. Configuration of test engine and specification of the test injector. (a) Configuration, (b) swirl injector.

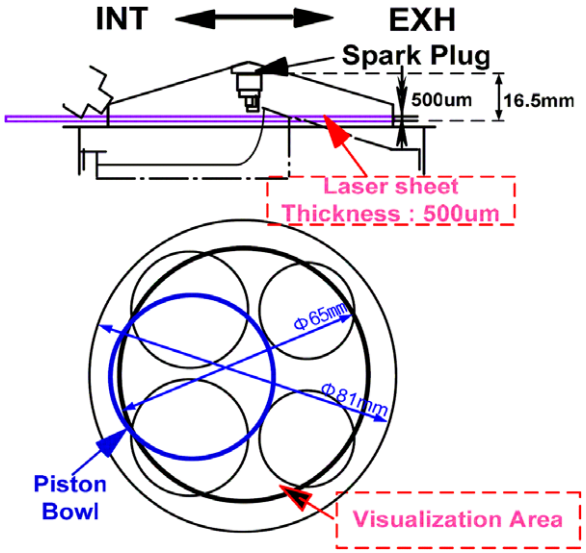

Fig. 4. Schematic diagram of the visualization region at compression stroke.

were installed at the top of the cylinder head gasket. The piston head was modified and transparent.

The schematic diagram of the visualization region at the late injection mode is shown in Fig. 4. The laser sheet beam was located 2 mm at the bottom of spark plug. Using this system, we analyzed the fuel stratification characteristic near the spark plug in accordance with variable injection timing as the ignition timing is BTDC 20°.

2.2. Analysis method

2.2.1. Cross-correlation particle image velocimetry

The PIV is now a well established technique for the measurement of instantaneous planar velocity fields and has

been reviewed by a number of authors [1–5]. In its simplest form, the flow is illuminated with a double pulsed light sheet and the positions of tracer particles are recorded with a photographic camera viewing normal to the plane of the sheet. The mean particle displacement vector in each small region of the flow is determined by performing a spatial correlation of the particle image field in that region. If the image is a simple double-exposure, then autocorrelation analysis is used. If the first and second particle image fields can be recorded separately, the more robust cross-correlation interrogation methods may be used [12,14,18]. This gives the important benefits of improved measurement dynamic range, better tolerance to velocity gradients and seed concentration variations and elimination of directional ambiguity. The photographic recording of a high-speed time series of moving particle fields for cross-correlation PIV has been reported for combustion studies in constant volume vessels [26] and also in cycle-resolved engine studies [32]. It has been shown by practitioners of digital PIV that, depending on the details of the flow structure, reasonable accuracies may be achieved by using interrogation region dimensions as low as 16×16 pixels, with the condition that particle images occupy no less than 2×2 pixels [2,4,8,15]. Thus, the possibility exists of generating velocity measurements on a regular grid of 16×16 locations with a 50% overlap each calculated using an FFT-based cross-correlation of a 16×16 pixel interrogation region over an image field of 128×128 pixels. This resolution is adequate for the characterization of the large-scale flow structures encountered in typical IC engines after inlet valve closure and before the rapid flow distortion is encountered in the last stages of compression. The available resolution may be used to study a large region with a relatively sparse measurement grid or a PIV probe system could alternatively be used to measure flow to higher spatial resolution or accuracy in smaller regions [4,6,13,17].

Seeding particles are introduced into the flow in order to reveal the motion of the gas. They must be present and accurately follow the flow, while scattering sufficient light to be detectable. The inertia of particles affects how well they respond to changes in spray and air velocity and in general impose the condition that particles are small. This experiments is able to produce (and hence to use in the PIV System) polystyrene particles, whose diameter is about 20 μm.

The present study recorded particle images exposed by each sequential laser beam at separate frames by using a CCD camera and calculated the velocity vector using a cross-correlation PIV algorithm. The direction of the particle velocity vector was determined clearly because the particle images of each laser pulse were recorded at separate frames. Fig. 5 shows the 'frame-straddling' method, which aligns a laser pulses at each sequential CCD camera frames. Fig. 6 shows the cross-correlation PIV algorithm using fast Fourier transform (FFT), which is programmed to obtain the velocity by calculating the coordinates of the location of the maximum cross-correlation parameter.

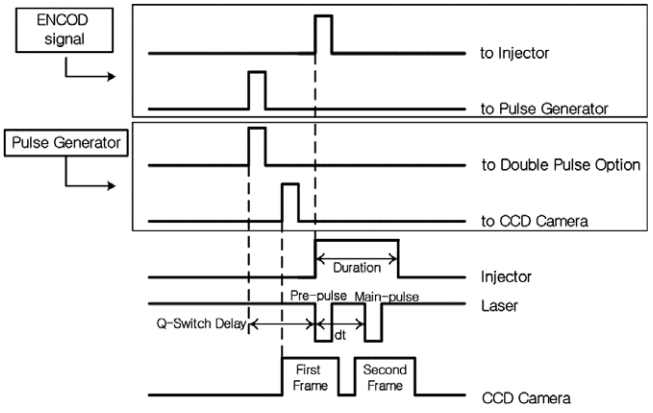

Fig. 5. Schematic diagram of frame straddling and timing chart.

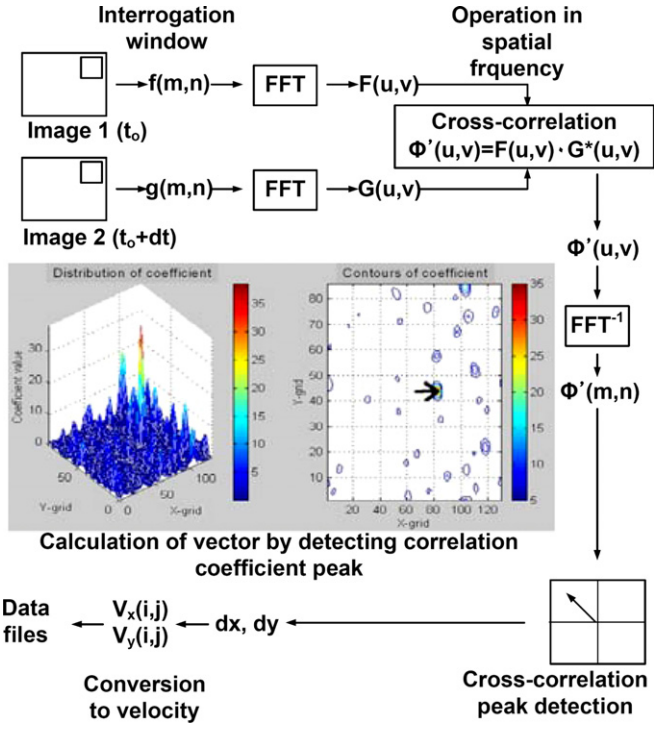

Fig. 6. Schematic diagram of the cross-correlation PIV algorithm.

2.2.2. Verification of PIV algorithm by a standard image

For the calculation of the velocity field, the PIV uses data of area observation instead of that of point observation, which is used by previous methods. Therefore, the PIV can measure the velocity field at a certain instant quantitatively, and is widely used in the study of turbulent or unsteady flow [1,4]. However, as the experimental apparatus and the analysis algorithm are developed, each researcher uses different apparatus and different algorithms to increase the accuracy. To establish a standard PIV many studies are performed throughout the world. One of the studies is the project of JPIV (PIV-STD project) that is held by the Visualization Society of Japan. The project evaluated efficiency and accuracy of a PIV system and established the PIV standard for analyzing algorithm.

The present study evaluated the accuracy of the developed PIV algorithm with the standard images suggested by JPIV. Fig. 7(a) shows one of four sequential reference images downloaded by the Visualization Society of Japan, and Fig. 7(b) shows the velocity field of the image calculated by the program of the present study. The specification of standard images is shown in Table 4, and the compared results of calculated vector on standard images are shown in Table 5. The calculated average velocities show lower values than the standard with the error of 2%. This is because when we divide the image area into small interrogation areas, we divide the size of interrogation areas too small. Determining the optimal size of the interrogation areas is important because the total velocity field shifts down as the size of the interrogation area becomes smaller. The present study determined the size of the interrogation area by the usually accepted one-quarter rule, which is suggested by Adrian. The rule recommends determining the size of the interrogation area as four times the average particle moving distance. By the verification using the standard images, we can confirm that the velocity field can be obtained by the present PIV system with the uncertainty of 2%.

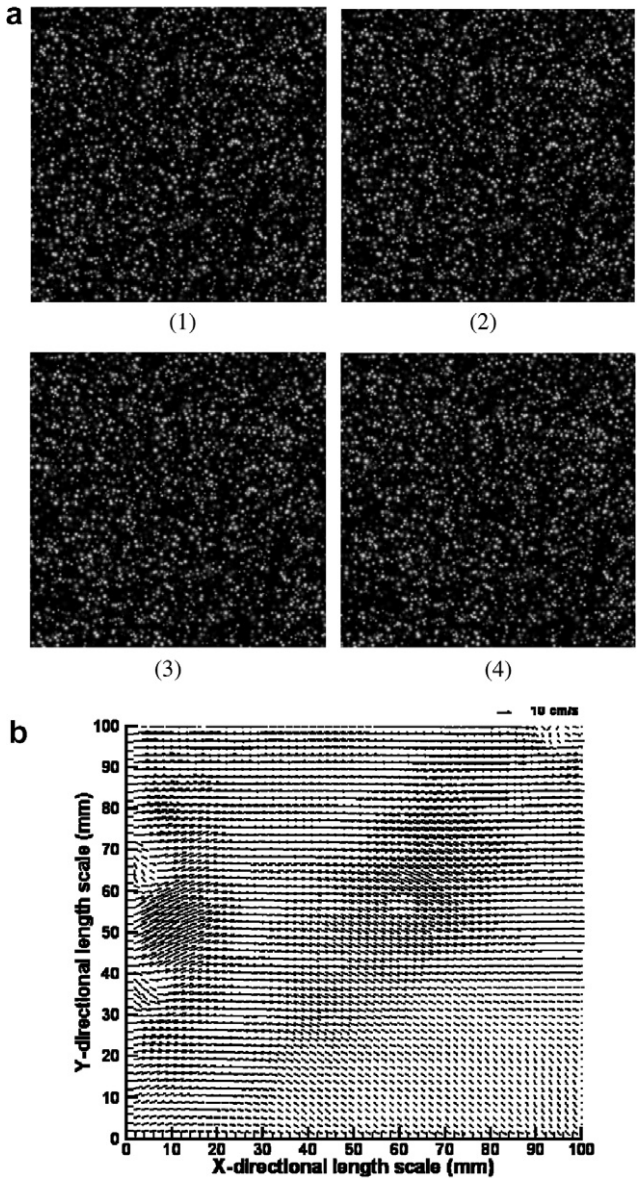

Fig. 7. Standard image and calculated velocity distribution. (a) standard image, (b) velocity distribution.

Table 4
Specification of standard images

Specification	Value	Unit
Image size	256×256	pixel
Area	10×10	mm
Laser thickness	2	mm
Interval	0.033	s
Average velocity	8.9	cm/s
Particle displacement (average)	7.5	pixel/interval
Particle displacement (standard deviation)	3.0	pixel/interval
Particle displacement (maximum)	15.0	pixel/interval
Number of particle	4000	–
Particle diameter (average)	5.0	pixel
Particle displacement (standard deviation)	1.4	pixel

Table 5
Compared results of calculated vector on standard images

Correlating images	Particle displacement 7.5 (pixel/interval)		Average velocity 8.9 (cm/s)	
	Value	Error (%)	Value	Error (%)
1 & 2	7.402	1.254	8.768	1.473
2 & 3	7.352	1.972	8.792	1.212
3 & 4	7.384	1.791	8.720	2.014

2.2.3. Principle of vorticity measurement

The vorticity field, ω, is an important Gallilean invariant vector field. Each of the vorticity components can be computed from the corresponding measured in-plane velocity vector field data using it is the basic definition [6,16].

$$\omega = \nabla \times \vec{u} \tag{1}$$

where $\vec{u}$ is the velocity field. This paper is concerned with the measurement of one component, denoted by ω_z which points in the positive Z-direction of an X–Y–Z Cartesian coordinate frame.

$$\omega_z = \frac{\mathrm{d}v}{\mathrm{d}X} - \frac{\mathrm{d}u}{\mathrm{d}Y} \tag{2}$$

where u and v are the velocity components in the X-direction and Y-direction of the X–Y–Zcoordinate frames, respectively. The results derived in this paper apply equally well to the remaining vorticity components ω_x and ω_y that point in the X-direction and Y-directions respectively.

In this study, we used the Ossen vortex algorithm. Using the synthetic u and v velocity arrays derived from Ossen expression [28], the synthetic vorticity arrays was numerically generated. Two prevailing techniques were evaluated. First, synthetic vorticity was calculated using a simple difference equation the standard vorticity algorithm in

NASA's 3-D plotting software, as well as TSI's post-processing software. The data shows (see Fig. 8).

$$\omega_{i,j} \cong \frac{1}{\Delta L}\left[\frac{U_{i,j-1}-U_{i,j+1}}{2}+\frac{V_{i+1,j}-V_{i-1,j}}{2}\right] \tag{3}$$

where, L means the length of the arrogation area.

Second, numerical vorticity was calculated using an eight-point circulation vorticity equation taken from Reuss et al.

$$\omega_5 = \frac{\Delta L}{(2\Delta L)^2}\left[\begin{array}{c}(u_2-u_8)+(u_6-u_4)\\ +0.5\left(\begin{array}{c}(u_3-u_9)+(u_1-u_7)\\ +(u_9-u_7)+(u_3-u_1)\end{array}\right)\end{array}\right] \tag{4}$$

Finally, most textbooks on numerical methods point out that higher order techniques provide higher accuracy because the order of approximation is improved. This does not necessarily hold true for noisy data, however, and so we have tested on the second order, the central difference approximation given by ref [28] in order to ascertain how our techniques affected the estimator given here

$$\omega_{13} = \frac{1}{\Delta L}\left[\begin{array}{c}\frac{(v_{11}-v_{15})+(u_3-u_{23})}{12}\\ +\frac{8(v_{14}-v_{12})+8(u_{18}-u_8)}{12}\end{array}\right] \tag{5}$$

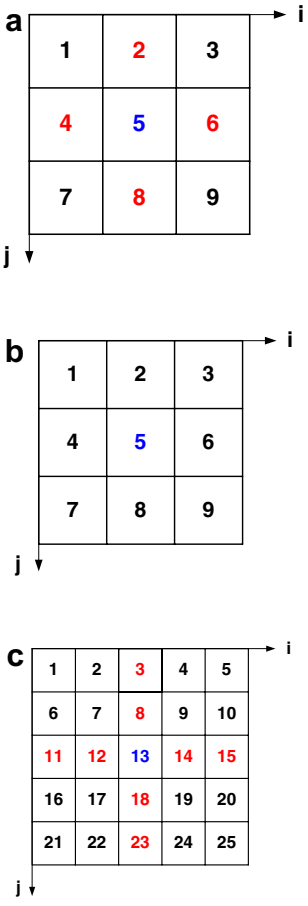

Fig. 8. Schematic of sampling by the vorticity estimator presented in Eqs. (3)–(5) [28]. (a) Simple difference, (b) eight-point circulation, (c) second order central difference.

This is one of several second order approaches one could adopt. A central difference scheme is the most appropriate for comparison to the other first order estimators.

2.2.4. Entropy analysis

The entropy analysis of the laser scattering images is based on the concept of statistical thermodynamics [31]. Boltzmann studied the correlation between the probability of particle distribution in the control volume and the entropy. If the particle number of N_i exists in energy level ε_i, the number of possible combinations (W) of the total particles number N. This is expressed as

$$\begin{aligned} W &= {}_N C_{N_1} \times {}_{(N-N_1)} C_{N_2} \times \cdots \times {}_{N_M} C_{N_M} \\ &= \frac{N!}{N_1!N_2!N_3!\cdots N_M!} = \frac{N!}{\prod N_i!} \end{aligned} \tag{6}$$

The entropy might be expressed in the natural logarithm of W combination, according to the concept of Boltzmann's statistics. When the Stirling approximation is applied to the case of $n \gg 1$, the natural logarithm of W is expressed as

$$\begin{aligned} &\ln n! \approx n\ln n - n \quad (n \gg 1) \\ &\ln W = \ln N! - \sum \ln N_i \\ &\quad = N\ln N - N - \sum N_i \ln N_i + \sum N_i \\ &\quad = N\ln N - \sum N_i \ln N_i \end{aligned} \tag{7}$$

$$\begin{aligned} S &= k\ln(W) \\ &= k\left[N\cdot\ln(N) - \sum\{N_i\cdot\ln(N_i)\}\right] \end{aligned} \tag{8}$$

where, S is the entropy and k is a Boltzmann constant.

If the number of particles in each cell of the image, N_i, is assumed to be proportional to the image intensity of the cell, $I_{(i)}$, the entropy can be expressed as

$$S = \alpha\cdot\left\{\sum_i^M I_{(i)}\right\}\cdot\ln\left\{\sum_i^M I_{(i)}\right\} - \alpha\cdot\sum_i^M[I_{(i)}\cdot\ln\{I_{(i)}\}] \tag{9}$$

where M is the number of cells in the image and α is a figure including a Boltzmann constant and the proportional coefficient between the number of overall particles and the image intensity.If the particle is assumed to be uniformly scattered, the average intensity is

$$\overline{I_{(i)}} = \frac{1}{M}\cdot\sum_i^M I_{(i)} = \frac{I_t}{M} \tag{10}$$

where I_t is the integrated value of the image intensity over the whole image area. The entropy of a homogeneous divergence is then

$$S_1 = \alpha\cdot I_t\cdot\ln(M) \tag{11}$$

The image intensity is divided between 0 and 255, with the total image intensity kept constant. So the entropy S_0, obtained from the divided image intensity, is calculated as

$$S_0 = \alpha\cdot[I_t\ln(I_t) - PI_t\cdot\ln(I_{\mathrm{MAX}})] \tag{12}$$

Where, P is the number of cells that gray light 255 occupy.

The normalized entropy S^* can be defined as

$$S^* = \frac{S - S_0}{S_1 - S_0} = \frac{I_t \ln(I_{MAX}) - \sum_i^M \{I_{(i)} \cdot \ln(I_{(i)})\}}{I_t \cdot \{\ln(M) - \ln(I_t) + \ln(I_{MAX})\}} \quad (13)$$

The homogeneity degree of the spray and the diffusion phenomena [27,29,30] can be analyzed by normalized entropy.

2.2.5. Verification of entropy analysis

For the verification of the entropy analysis method, the entropy analysis is performed to the images of water particles coming out of a humidifier. Fig. 9(a) is the image upstream near the exit nozzle of the humidifier, and Fig. 9(b) is the image downstream 20 cm distance from the nozzle. The size of the images is 150×150 pixels. Because the water particles come out from the small nozzle of the humidifier and spread to the surrounding area, the image downstream shows more homogeneous particle distribution than the image upstream. From the basic concept of the entropy, the entropy at the downstream point should be higher than that at the upstream point. The results of entropy analysis show higher entropy downstream as shown in Table 6.

Fig. 10 is the comparison of the images of circles with different sizes, numbers, sharpness and gray scales but with the same total image intensities. The entropy is zero when all particles are located at one point, and it increases as the particles propagate to the surrounding area. Comparing image 1 and image 2 in Fig. 7, image 2 is the image of the greater particle propagation, because image 2 has a wide spread uniform strength of large circle while image 1 has circles with particles concentrated at the center of the circles. Comparing image 2 and image 3, image 3 is the image of the propagation more progressed because it has a larger circle. The results of entropy analysis show the same results as shown in Table 6. From the entropy analysis of Figs. 9 and 10, the normalized entropy calculated by Eq. (13) has a larger value as the image strength is distributed more uniformly and more homogeneously throughout the whole area of the image. Therefore, it can be verified that the homogeneity degree of the measurement area can be calculated by the entropy analysis, and the diffusion strength of the spray can be measured quantitatively from the variation of entropy.

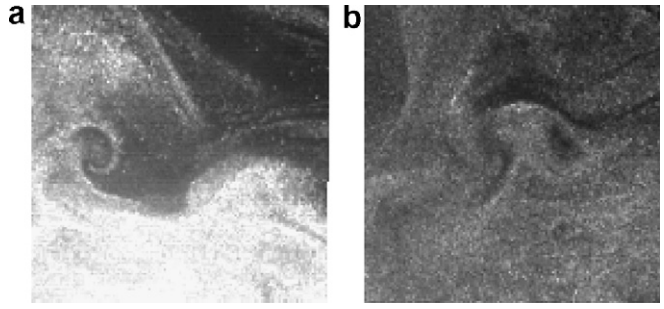

Fig. 9. Comparison of apparently different particle distributions. (a) Upstream, (b) downstream.

Table 6
Results of the entropy analysis for test images

Pictures	Figure No.	Normalized entropy S^*
Upstream	Fig. 9(a)	0.822
Downstream	Fig. 9(b)	0.973
Image 1	Fig. 10(a)	0.288
Image 2	Fig. 10(b)	0.339
Image 3	Fig. 10(c)	0.460

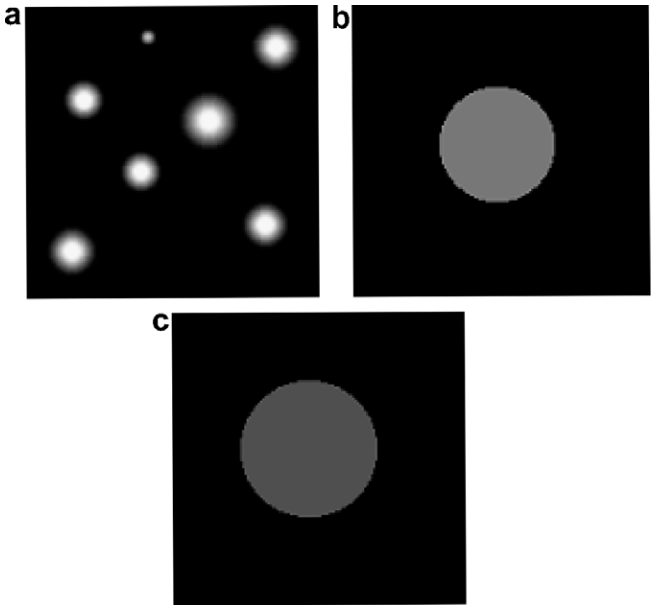

Fig. 10. Comparison with different size, number, sharpness and gray scale of circles in same total image intensity. (a) Image 1, (b) image 2 (c) image 3.

3. Results and discussion

3.1. Flow characteristic in the cylinder

A straight port performance engine block was used in this study. Fig. 11 shows the result of the valve lift in accordance with the variable crank angle.

3.2. Flow velocity distribution in cylinder

Fig. 12 shows the results obtained for the flow velocity in the cylinder in accordance with changing the crank angle or valve lift for the intake stroke as the number of rotations is 600 (rpm). It calculated the flow velocity from ATDC 90° to ATDC 150° by 20 °CA. As shown in Fig. 11, it found that the maximum intake flow rate is 130 °CA. From the results, the flow entered intake port separates toward both walls and in the cylinder occurs at the reverse tumble flow

due to the shape of the intake port. The reason for this is the performance of the intake port. The velocity of the left side is trong but that of right side is diminished. In the case of the commercial port, that of the right side is strong. Accordingly, as the crank angle increases, the velocity of the left side is active; then after ATDC 150°, it is inactive. But the velocity of the right side diminishes gradually in

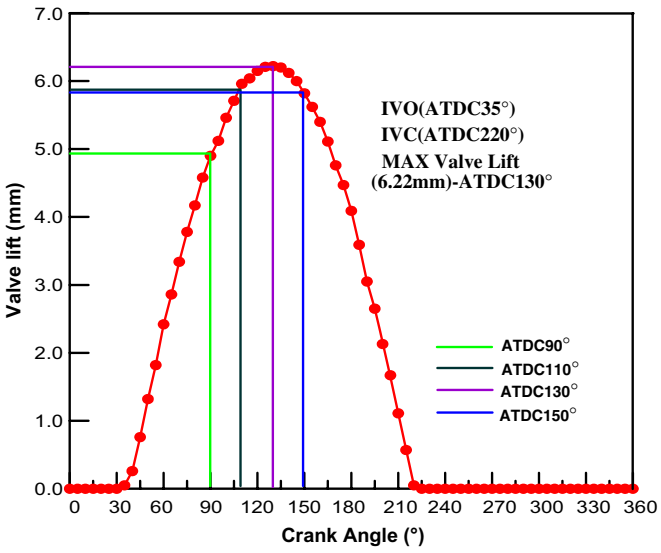

Fig. 11. Variation of the valve lifts in accordance with the crank angle.

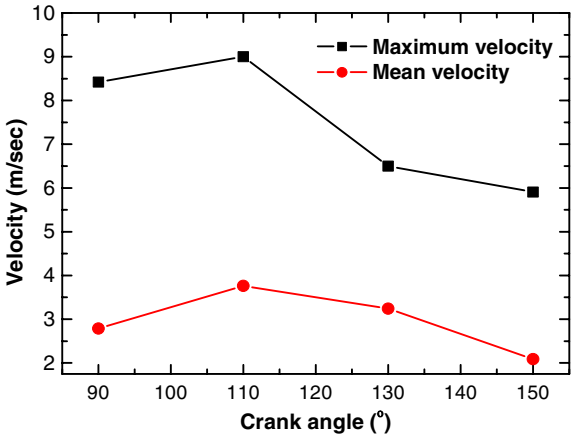

Fig. 13. Average velocity according to crank angle.

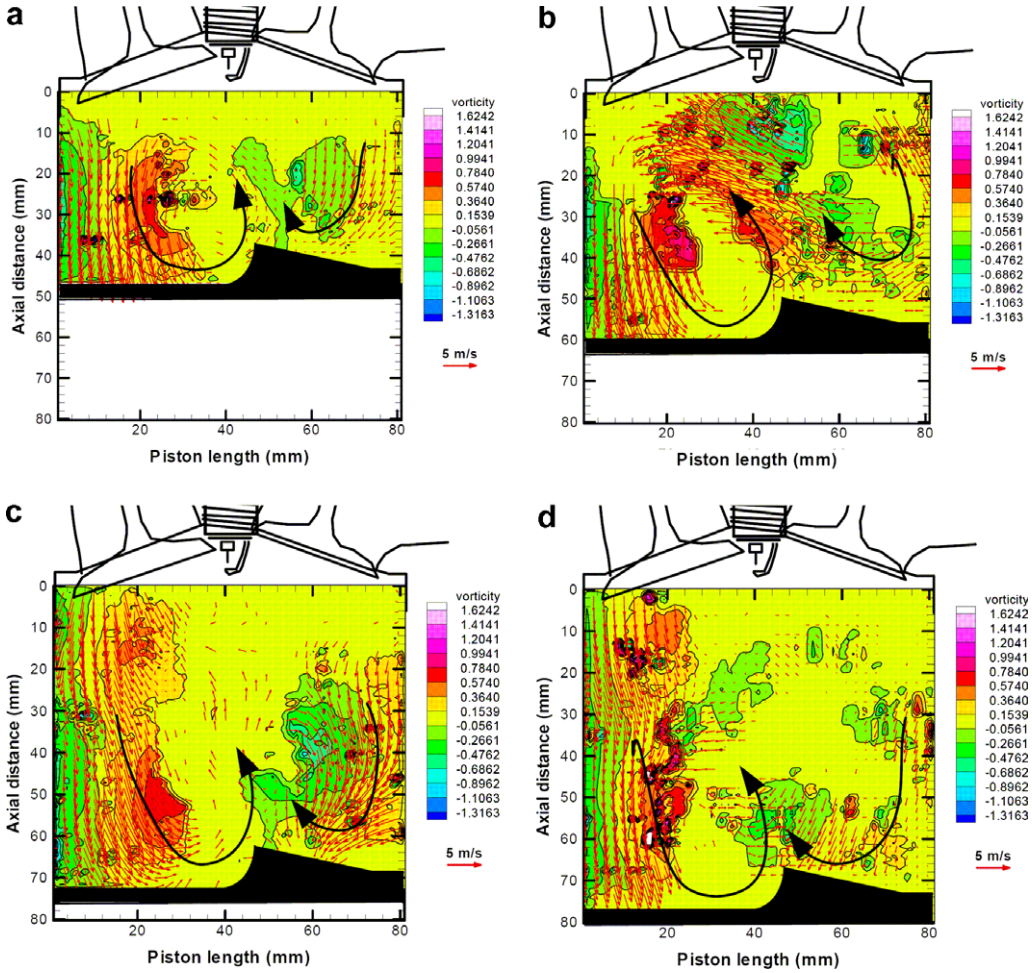

Fig. 12. The velocity and vorticity distribution in accordance with crank angle at intake stroke: (a) ATDC 90°, (b) ATDC 110°, (c) ATDC 130°, (d) ATDC 150°.

accordance with the increasing crank angle. It is observed that the reverse collision tumble flow slightly decreased and then formed a vortex. As the crank angle increased, the vortex forming the interactive collision gradually decreased. It expects that the reverse tumble flow due to the intake flow has an effect on the homogeneous mixture distribution of the fuel droplet accompanied by the flow in the cylinder.

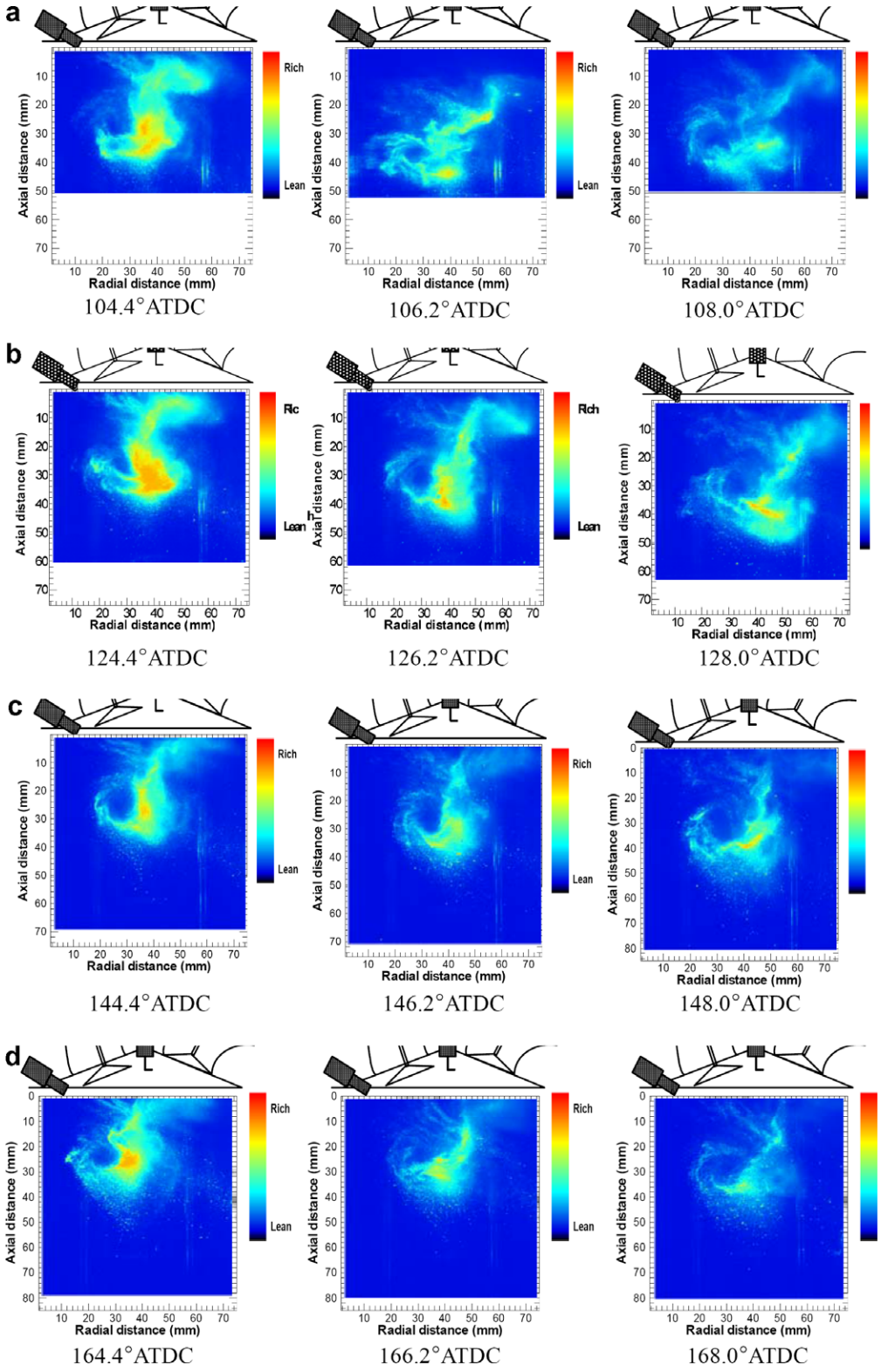

Fig. 14. Fuel mixture distribution in accordance with crank angle at intake stroke: (a) Injecting timing: 90° ATDC, (b) injecting timing: 110° ATDC, (c) injecting timing: 130° ATDC, (d) injecting timing: 150° ATDC.

3.3. Velocity in cylinder

Fig. 13 shows the results of maximum and mean velocity in accordance with the increasing crank angle using PIV technique as seen in Fig. 6. The strongest part of the velocity is the middle in the cylinder and then, as the crank angle is increased, the mean and maximum velocity in cylinder gradually decreases. As shown in Fig. 12, it found that the maximum average velocity in cylinder flow is 9 m/s, at 110° ATDC; as the crank angle increases, the mean velocity gradually decreases.

3.4. Fuel distribution using Mie-scattering method

Fig. 14 shows the fuel distribution in the cylinder in accordance with changing the injection timing using the Mie-scattering method. In the case of early injection timing, 90° ATDC, the fuel spay is attached to the wall-wetting piston crown. If it is injected at 90° ATDC, the engine will generate hydrocarbon. Through visual results, it found that the injection fitting timing is from 110° ATDC

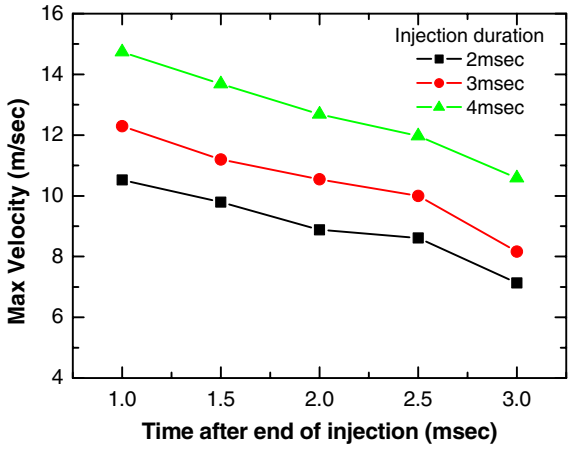

Fig. 16. The maximum velocity relative to injection duration.

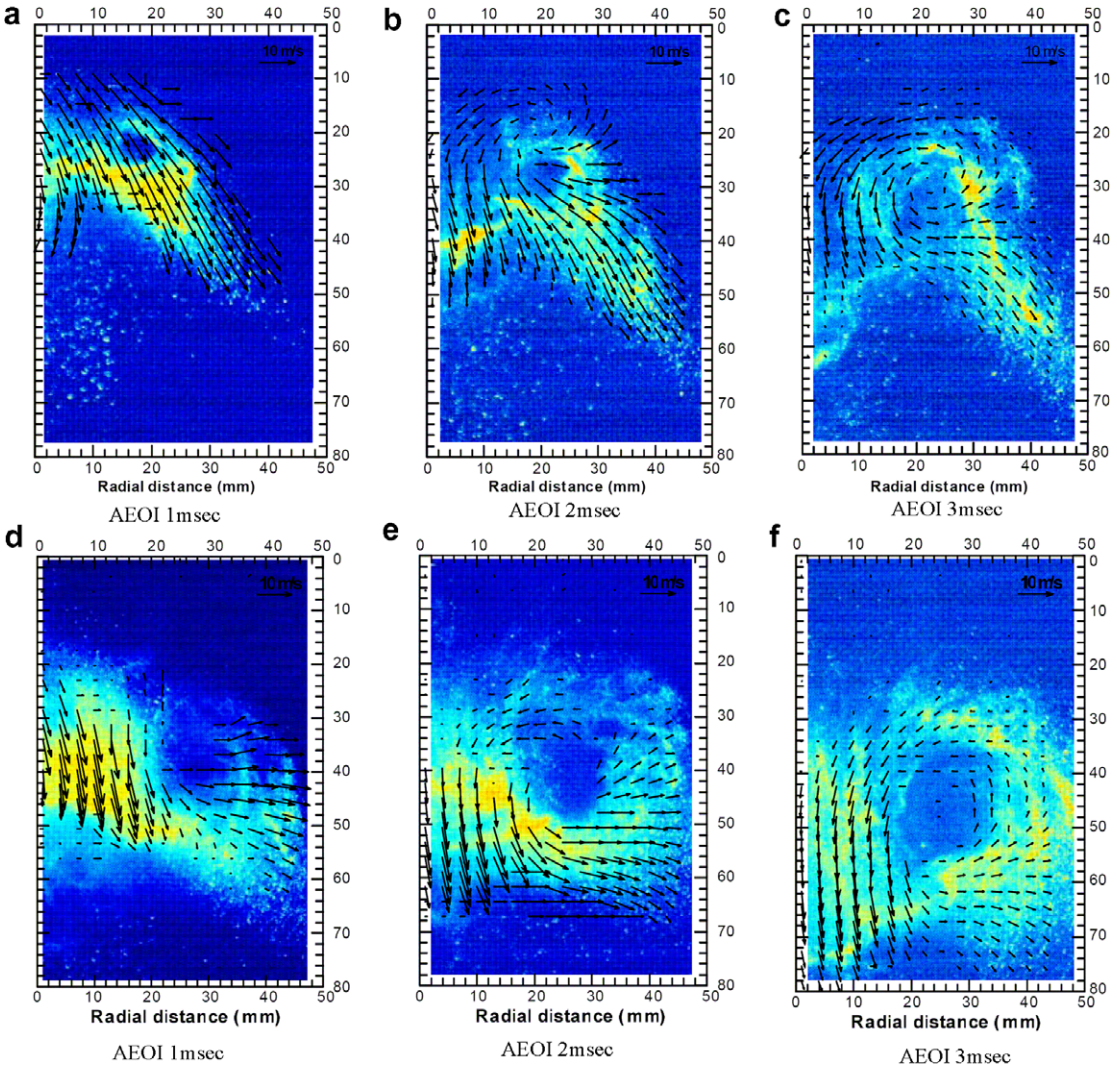

Fig. 15. The spray developing process and spray velocity distribution relative to injection duration ((a)–(c): 2 ms at injection duration, (d)–(f): 4 ms at injection duration).

to 130° ATDC. If it injected the injection timing at 150° ATDC, the spray injected from the injector is not involved in the reverse tumble flow, as seen in Fig. 12. Therefore, it found that if the timing of the injection is retarded after ATDC 130°, a homogeneous mixture distribution involving the intake air does not occur.

3.5. The velocity distribution of the fuel spray by using the PIV technique

3.5.1. Spray velocity to the free spray

Fig. 15 shows the velocity distribution of the vertical tomogram of the spray at 2 ms and 3 ms from the ignition

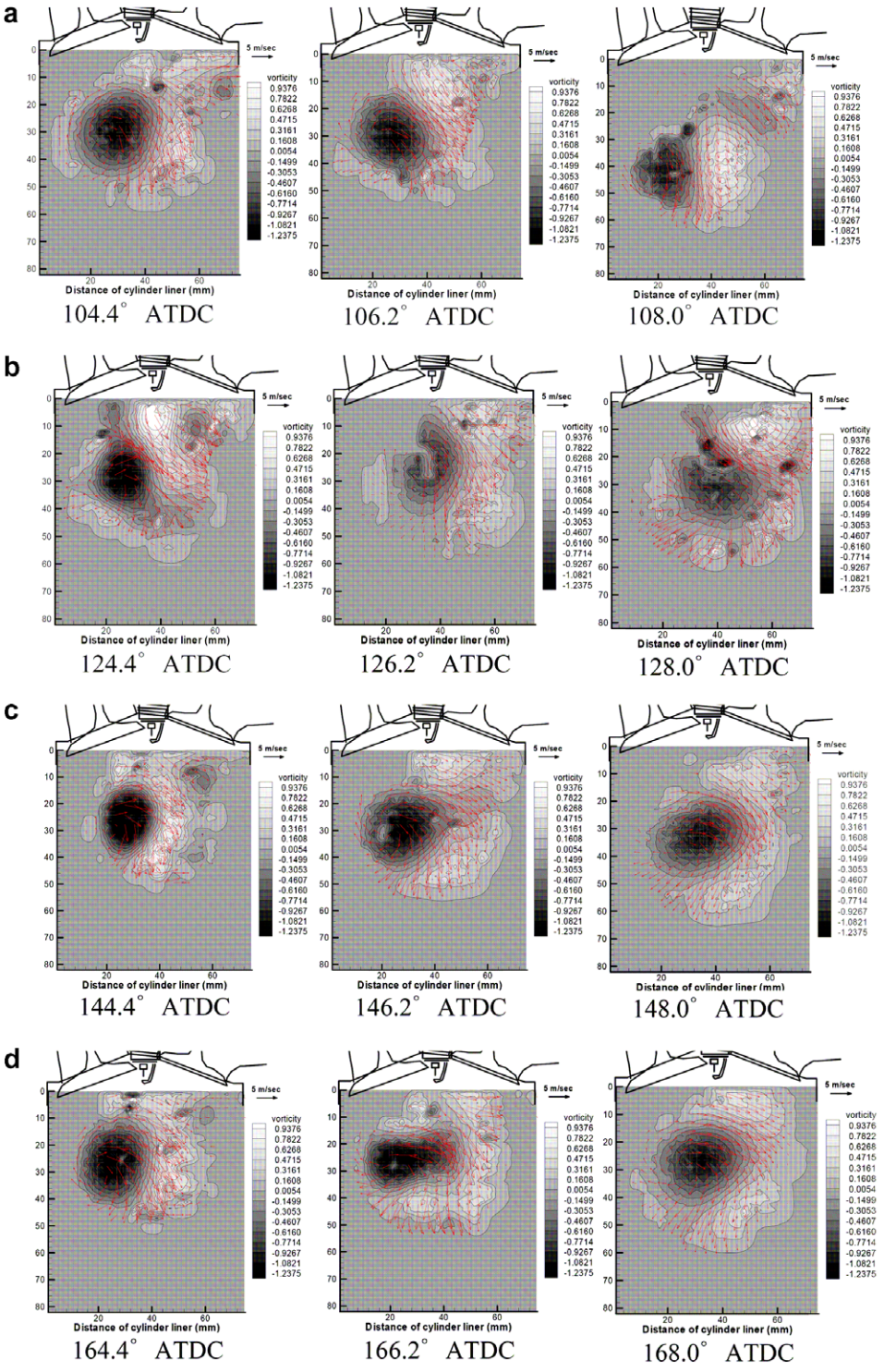

Fig. 17. The spray velocity and vorticity in accordance with changing injection timing. (a) Injecting timing: 90° ATDC, (b) injecting timing: 110° ATDC, (c) injecting timing: 130° ATDC, (d) injecting timing: 150° ATDC.

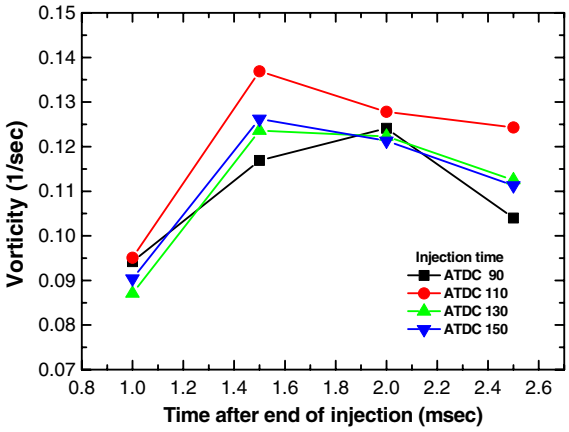

Fig. 18. The average vorticity in accordance with changing the injection timing.

of the injection at an ambient pressure of 0.1 MPa. The leading edge and central part of the spray shows relatively high velocity. Especially, although the velocity scale is small, a clear counter-rotating vortex motion is observed on the periphery of the spray. In particular, by carefully investigating the direction and scale of the velocity vectors in the spray periphery, the velocity vectors were found to indicate directly the negative axial direction in the axial distance of 20–30 mm with a small vortex scale in the case of the injection duration of 2 ms and 30–50 mm with a large vortex scale in the case of the injection duration of 4 ms.

Fig. 16 shows the maximum velocity in accordance with injection duration such as 2 ms, 3 ms, and 4 ms. As the injection duration is increased, the maximum velocity after the end of the injection in accordance with the elapsing timing is increased. The maximum velocity to injection duration is 10 m/s, at 2 ms, 12 m/s, at 3 ms, and 15 m/s, at 4 ms, respectively.

3.5.2. Spray velocity and vorticity distribution in the cylinder

Fig. 17 show the velocity and vorticity distribution of spray droplet in accordance with injection timing using the cross-correlation PIV technique and second order central difference method of the Ossen vorticity algorithm. Generally vortex is shown in the left and right but the vortex on right side is not observed in this result due to the intake flow. From the Fig. 12, as the velocity is high in case of 90–110° ATDC the location of the generated vortex moves to the middle direction of in cylinder and disturbs the spray velocity distribution. Also it found that the spray velocity is involved in the intake flow and the fuel spray is dispersed on the in cylinder homogeneously. In particular, investigating carefully examine the direction and scale of velocity vectors and vorticity strength in the cylinder, it is obseved that the velocity vectors indicate directly the negative axial direction in axial distance of 25–35 mm with ATDC 90–130° and about 20 mm with ATDC 150.

Fig. 18 shows the vorticity of the elapsing timing after injection. As seen in Fig. 17, when the injection time is at 110° ATDC, the vortex size is the largest. And in the case

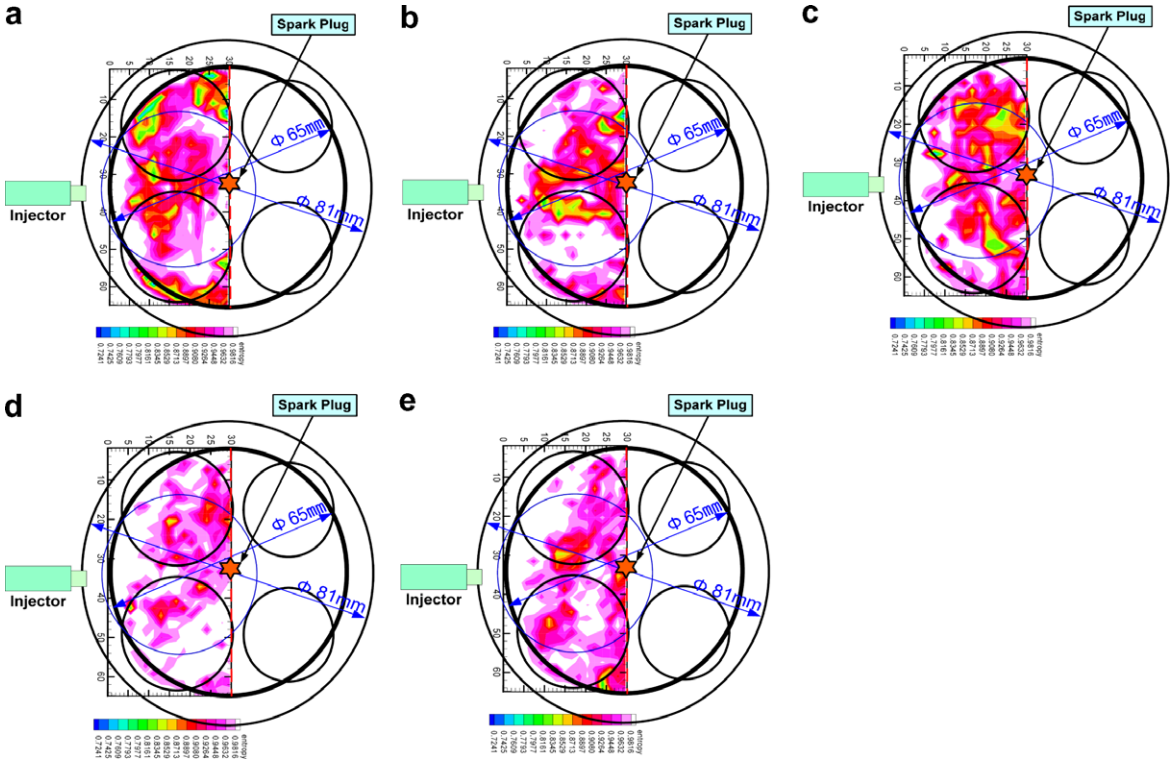

Fig. 19. The stratified characteristics relative to injection timing at the compression stroke using the entropy analysis: (a) 40° BTDC, (b) 50° BTDC, (c) 60° BTDC, (d) 70° BTDC, (e) 80° BTDC.

of 1.6 ms after the end of the injection (AEOI), the vorticity strength is highest at 110° ATDC. Finally, we found that this condition is optimized when involved in the intake flow and spray behavior of the visual engine.

3.6. The stratification effect of fuel with a compression stroke using entropy analysis

Fig. 19 shows the fuel stratification and mixture procedure using entropy analysis. The study is investigated on the entropy analysis of statistical thermodynamics to analyze quantitatively the diffusion of the mixture distribution and homogeneous and heterogeneity degree. The stratification effects near the spark plug at the compression stroke and set the injection timing from 40° BTDC to 80° BTDC at 10° CA intervals were observed. When the ignition timing was set to 20° BTDC, stratification near the spark plug in accordance with the injection timing in the late mode was observed and occurred. In the case of the injection timing at 50° BTDC and 60° BTDC, the stratification effect is higher than in other conditions. Near the spark plug, most of the heterogeneity is small scale of the entropy value and there are few large clouds. Far away the spark plug, the heterogeneities become unclear and the value of that is large scale. As the injection timing was slowed and speeded up, the stratified effect near the spark plug became less.

4. Conclusion

A new entropy analysis method based on statistical thermodynamics and the cross-correlation PIV measurement method has been developed. In this study, we understood the optimal conditions and characteristics through analysis of the stratification effect and the velocity field measurement of the cylinder.

By using the Mie-scattering method, entropy analysis, and particle image velocimetry, we observed the wall-wetting of the piston and the effect on the flow field in the cylinder in accordance with the fuel distribution and mixture homogeneous degree. Through this method, we found that the spray velocity is involved in the intake flow and the fuel spray is dispersed on the in cylinder homogeneously at an injection timing of 110° ATDC.

Based on the entropy concept of statistic dynamics, a method to analyze the homogeneity or heterogeneity degree of a field was developed as a tool to investigate phenomena in diffusion process. The homogeneous diffusion rate increased as the injection timing moved to the early intake stroke process, and BTDC 60° was the most efficient injection timing for the stratified mixture formation during the compression stroke. From the entropy analysis results, it is known that the spray is widely distributed according to the elapsed time after injection. Especially, in vaporization condition, entropy value is increased in a whole spray area from reference. Besides, as ambient pressure increases, the fuel distribution becomes heterogeneous condition. However, the temperature condition in case of the late injection is very high. The spray characteristics (entropy value is small scale) in case of the injection timing at 50° BTDC and 60° BTDC is the state of the heterogeneity which appears the low value of entropy. If this experiment is achieved in practical operating condition in actual engine, the temperature in cylinder become rise. We are expected that the mixture distribution near the spark plug change the heterogeneity to the homogeneity.

Acknowledgements

We would like to thank Combustion Engine Research Center (CERC) for financial support for this work.

References

[1] R.J. Adrian, Multi-point measurement of simultaneous vector in unsteady flow—review, Int. J. Heat Fluid Flow 7 (1986) 127–145.
[2] R.J. Adrian, Particle-imaging techniques for experimental fluid mechanics, Ann. Rev. Fluid Mech. 23 (1991) 261–304.
[3] C.E. Willert, M. Gharib, Digital particle image velocimetry, Exp. Fluids 10 (1991) 181–193.
[4] T. Urami, R.F. Blackwelder, A cross-correlation technique for velocity field extraction from particle visualization, Exp. Fluids 10 (1991) 213–223.
[5] A.M. Fincham, Low cost, high-resolution DPIV for measurement of turbulent fluid flow, Exp. Fluids 23 (1997) 449–462.
[6] L. Lourenco, A. Krothapalli, On the accuracy of velocity and vorticity measurements with PIV, Exp. Fluids 18 (1995) 421–442.
[7] A. Fouras, J. Soria, Accuracy of out-of-plane vorticity measurements derived from in-plane velocity field data, Exp. Fluids 25 (1998) 409–430.
[8] J. Westerweel, Digital particle image velocimetry—theory and application Ph.D. Thesis, Technical University of Delft, 1993.
[9] Gong Xin-Shen, On the approach to ideal observation and measurement techniques for fluid mechanics (and introduction of some recent work at BUAA), in: Proceedings of the SPIE—The International Society for Optical Engineering 3172, 1997, pp. 540–550.
[10] J. Westerweel, Fundamentals of digital particle image velocimetry, Measure. Sci. Technol. 8 (12) (1997) 1379–1392.
[11] R.J. Adrian, Dynamic ranges of velocity and spatial resolution of particle image velocimetry, Measure. Sci. Technol. 8 (12) (1997) 1393–1398.
[12] J. Westerweel, D. Dabiri, M. Gharib, The effect of a discrete window offset on the accuracy of cross-correlation analysis of digital PIV recordings, Exp. Fluids 23 (1) (1997) 20–28.
[13] H. Huang, D. Daibiri, M. Gharib, On errors of digital particle image velocimetry', Measure. Sci. Technol. 8 (12) (1997) 1427–1440.
[14] -H. Huang, An extension of digital PIV-processing to double-exposed images, Exp. Fluids 24 (4) (1998) 364–372.
[15] J. Nogueira, A. Lecuona, P.A. Rodriguez, Data validation, false vectors correction and derived magnitudes calculation on PIV data, Measure. Sci. Technol. 8 (12) (1997) 1493–1501.
[16] L. Lourenco, A. Krothapalli, On the accuracy of velocity and vorticity measurements with PIV, Exp. Fluids 18 (6) (1995) 421–428.
[17] L. Gui, W. Merzkirch, A method of tracking ensembles of particle images, Exp. Fluids 21 (6) (1996) 465–468.
[18] J. Westerweel, Effect of sensor geometry on the performance of PIV interrogation, in: 9th International Symposium on Applications of Laser Techniques to Fluid Mechanics. July 1998, Lisbon, Portugal.
[19] Y. Takagi, T. Teruyuki, et al., Simultaneous attainment of low fuel consumption, high ourput power and low exhaust emissions in direct injection si engine, SAE 980149, 1998.

[20] F.Q. Zhao, M.C. Lai, A review of mixture preparation and combustion control strategies for spark-ignited direct-injection gasoline engine, SAE 970627, 1997.
[21] H. Michael, A. Brad et al., Early spray development in gasoline-direct-injected spark ignition engine, SAE 980160, 1998.
[22] C. Preussner, C. Döring, et al., GDI: interaction between mixture preparation, combustion system and injector performance, SAE 980498, 1998.
[23] Y. Iwakiri, A. Kakuho, et al., Effectiveness and issues of various measurement techniques used in evaluating spray characteristics in a direct-injection gasoline engine, in: Proceeding of The 15th International Combustion Engine Symposium, 9935095, 1999.
[24] F.-Q. Zhao, J.-H. Yoo, M.-C. Lai, et al., Spray dynamics of high-pressure fuel injectors for DI gasoline engines, SAE 961925, 1996.
[25] T. Kume, Y. Iwamoto, et al., Combustion controlled technologies for direct injection si engine, SAE 960600, 1996.
[26] M. Yamakawa, S. Isshiki, T. Yoshizaki, K. Nishida, et al., Measurement of ambient air motion of DI gasoline spray by LIF-PIV, Comodia (2001) 499–504.
[27] R. Yuyama, T. Chikahisa, K. Kikuta, Hishinuma, Entropy analysis of microscopic diffusion phenomena in diesel sprays, Comodia (2001) 542–550.
[28] J.D. Luff et al., Experimental uncertainties associated with particle image velocimetry based vorticity algorithms, Exp. Fluids 26 (1999) 36–54.
[29] T. Chikahisa, R. Yuyama, K. Kikuta, Y. Hishinuma, Entropy analysis of microscopic diffusion phenomena in diesel sprays, JSME Int. J., Ser. B 46 (1) (2003) 109–116.
[30] T. Chikahisa, Entropy method for analyzing heterogeneity degree in diffusion process (basic concept and application results for microscopic structure in sprays), Transaction of SAE, 2004-01-1964.
[31] Ikeda, Toukei netsu rikigaku, Statistic thermodynamics, Kyoritsu book Co., pp. 9–23.
[32] M. Reeves, D.P. Towers, B. Tavender, C.H. Buckberry, Technique for routine, cycle-resolved 2-D flow measurement and visualization within SI engine cylinders in an engine development environment, in: 10th International Symposium on Applications of Laser Techniques to Fluid Mechanics, Lisbon, 2002, 10–13 July, paper 22.2.